Tailored copper oxidation in alkaline aqueous solution after helium cation implantation

Subing Yang, Yuki Nakagawa, Tamaki Shibayama*

Faculty of Engineering, Hokkaido University, Sapporo, Hokkaido 060-8628, Japan

* Corresponding author.

E-mail address: shiba@qe.eng.hokudai.ac.jp

Abstract

Manipulating Cu oxidation is important for Cu anti-oxidation techniques and Cu oxide fabrication. In this study, Cu oxidation behavior after He^+ implantation was observed after exposure to 0.1 M aqueous NaOH, and the underlying microstructural evolution and mechanism were investigated. He^+ implantation and some C concomitantly introduced into the Cu surface accelerated formation of a thin oxide layer during the initial oxidation period, resulting in faster initial generation and more rapid growth of CuO during the subsequent oxidation. Furthermore, He^+ implantation homogenized the distribution of CuO on the Cu substrate. Our findings will increase researchers' understanding of the oxidation and corrosion behavior of Cu in aqueous alkaline conditions, and provide new insights into designing and growing Cu oxide nanostructures by ion implantation.

Keywords: helium ion implantation; copper oxidation; copper oxide nanostructure.

Introduction

As one of the most important metals, Cu is widely used in various industrial components (such as pipes and valves) as well as electrical systems and electronic devices; this wide use is due to its high thermal and electrical conductivities, ductility, and overall nontoxicity [1,2]. However, Cu readily oxidizes after several working cycles, even at room temperature; this oxidation impacts its performance in industrial and technological applications. Although many anti-oxidation techniques have been developed (such as alloying; electroplating; and surface-passivation technologies by using organic molecules, inorganic materials, or carbon-based materials as oxidation inhibitors [1,3]), applying these techniques has various drawbacks and limitations. For example, alloying with Cr or Ni degrades the thermal and electrical properties of Cu [4], and oxidation inhibitors often have limited success in large-scale applications [1,3]. However, two forms of Cu oxide [Cu(I) oxide (Cu_2O) and Cu(II) oxide (CuO)] are excellent semiconductors that have a narrow band gap; and have drawn great interest in terms of their applications in catalytic, gas sensor, optoelectronic, and solar technologies. These Cu oxides can be

prepared by many methods (such as chemical and electrochemical deposition [5], anodization [6], and electrostatic spray deposition [7]). Furthermore, many methods have been exploited to design or fabricate specific copper oxides. For example, Ma et. al. [8] reported that an aligned two-dimensional single-crystal Cu_2O film can be deposited onto a Cu substrate by the polyol method. F-doped SnO_2 glass [9], TiO_2 nanotube arrays [10], and other materials have been used as substrates for growing Cu oxide nanostructures [11]. However, to date, the development of commercially viable copper oxides for photocatalysis, sensors, and solar-driven water-splitting remains challenging. Therefore, there is two-fold interest in Cu oxidation: mitigate Cu oxidation against technological failure, and exploit potential corresponding industrial applications; both lines of inquiry require manipulation of Cu oxidation.

It is generally accepted that oxidation and corrosion behavior corresponds to surface properties, which can be modified by surface treatment [2]. Ion implantation has been investigated to improve surface oxidation resistance by selectively implanting alloying elements. The nature of ion implantation facilitates introduction of any element into the

near-surface region of a solid in a controlled and reproducible manner [12], which is independent of most equilibrium constraints [13]. Ion implantation has been reported to improve the corrosion resistance of nickel [14] and stainless steel [15], aluminum alloy [16] and nickel–aluminum bronzes [17]. Moreover, Zhao et al. [4] reported that a shallow implantation of Cr, Al, and Mg can enhance the oxidation resistance of Cu films and does not substantially affect the films' conductivity. C is usually introduced onto the surface concomitantly with the implanted ion due to the pump oil within the vacuum system [18,19]. In our recent studies of He^+ implantation on Cu [20], C was implanted into Cu to a depth of several nanometers concomitantly with He^+ ions; doing so passivated the Cu thermal oxidation by forming a barrier layer that blocked contact of Cu with air. An alkaline environment readily oxidizes or corrodes Cu, and has been widely investigated for anti-oxidation of Cu and Cu oxide growth [12,21-24]. Because of the C-containing layer induced by He^+ implantation [20], He^+-implanted Cu is also expected to impart passivation to oxidation in an alkaline environment. However, in this study, it is found that Cu implanted with He^+ exhibited enhanced CuO generation in alkaline aqueous solution,

rather than the expected passivation of oxidation. Furthermore, He^+-implantation causes a relatively ordered configuration of CuO on the Cu substrate. The aim of this study was to clarify this oxidation behavior of Cu in alkaline aqueous solution after He^+ implantation. In this context, the morphology and microstructural evolution of Cu after oxidation was investigated by various microscopy techniques. A thin oxide layer rapidly formed on He^+-implanted Cu after immersion in alkaline aqueous solution, subsequently resulting in faster initial generation and more rapid growth of CuO. These results will increase researchers' understanding of the oxidation and corrosion behavior of Cu in alkaline aqueous conditions, and provide new insights into designing and growing Cu oxide nanostructures.

2. Materials and Methods

2.1. Materials and ion implantation

Polycrystalline Cu (99.99%, size 10 mm × 10 mm × 1 mm) was purchased from Nilaco Corporation (Tokyo, Japan, No. 1054). NaOH was purchased from FUJIFILM Wako Pure Chemical Corporation (Osaka, Japan, No. 19818863). The surface of Cu was polished with #2000 emery

paper, followed by mechanically polishing to a mirror plate with a buff grinder and 0.1 CR alumina as the polishing agent. Subsequently, each sample was mechanically polished for 10 min with a buff grinder and deionized water to remove any residual alumina. Finally, these samples were cleaned ultrasonically in acetone and deionized water sequentially 2× with each cleaning for 5 min, then rinsed with deionized water and dried in air.

He^+ implantation (100 keV) was performed on Cu substrates at room temperature to a fluence of 5.0×10^{15} cm^{-2} with an ion flux of 6.2×10^{12} cm^{-2} s^{-1}. Raster scanning with an ion beam was carried out to achieve homogeneous implantation with a vacuum greater than 1.0×10^{-5} Pa prior to implantation. After ion implantation, the He^+-implanted Cu was then cleaned with acetone and deionized water to remove the carbonaceous contamination that was absorbed onto the Cu surface during ion implantation [20]. The ion penetration profile of 100-keV He^+ was also calculated with SRIM 2013 software, in which the full damage cascade model was used (Fig. S1).

2.2 Cu oxidation

Aqueous NaOH (0.1 M) was prepared. Bulk Cu samples (with or without He^+ implantation) were immersed in 0.1 M aqueous NaOH at room temperature for various times; then the oxidation state of these samples was detected and analyzed.

2.3 Characterization

An optical microscope (Nikon Eclipse LV150) was used to record the surface and morphology variation of the samples. Raman analysis was carried out with a Raman microscope (HORIBA XploRA), equipped with a 532-nm-wavelength laser and a 2400-groove/nm grating. Raman spectra were obtained by confocal Raman microscopy with a confocal aperture of 100 μm. X-ray photoelectron spectroscopy (XPS) analysis (with a JEOL JPS-9200 spectroscope) was performed with a standard Al-Kα X-ray source, a measured size of 1.0 mm in diameter, and a pressure maintained at 10^{-7} Pa. Shirley-type background subtraction was performed before curve-fitting. XPS etching was used to analyze the sample composition in depth with 2-keV Ar^+ at an etching rate of about 2 nm/min, and an etching size of 3 mm × 3 mm.

The surface morphology of the sample was observed by field-emission

scanning electron microscopy (SEM; JEOL JSM–7001FA) at an accelerating voltage of 15 kV. A cross section of the bulk samples was made by using gallium ions in a focused-ion-beam (FIB) system (JEOL, JEM-90320FIB) at an accelerating voltage of 30 kV, which was then observed by SEM at a tilt angle of 70°. The transmission electron microscopy (TEM) samples were prepared by FIB at an accelerating voltage of 30 kV, and the samples were thinned to a final thickness of about 100 nm. To minimize the damage introduced into the TEM samples by gallium ions with the FIB system, these TEM samples were then polished by using low-energy Ar^+ with GentleMill (TECHNOORG-lINDA ltd. Co., Gentle Mill IV8 HI). Both sides of the TEM samples were polished at 1 kV, at 15°, for 3 min; and 0.3 kV, at 10°, for 20 min. The microstructure was observed with a JEOL JEM-2000FX at 200 kV. By using Cs-corrected scanning transmission electron microscopy (STEM; FEI, Titan G2 60-300), the high-resolution (HR) TEM and high-angle annular dark field (HAADF)–STEM analyses were carried out at an operation voltage of 300 kV.

3. Results and discussion

3.1 Modified surface morphology evolution

Upon analysis by SEM, no obvious variation in the surface morphology was observed on the sample after He^+ implantation (Fig. S2). However, after immersion in 0.1 M NaOH for 5 h, distinct differences were found between pristine Cu and He^+-implanted Cu, in terms of the surface morphology and oxidation products (Fig. 1). Regarding pristine Cu, some brown plaques were observed on the surface from the optical images [Fig. 1(a)]; these plaques are attributable to the oxide islands [Fig. 1(b)]. These oxide islands were randomly distributed with a size ranging from several tens to hundreds of nanometers, resulting in a rough surface. By Raman microscopy [Fig. 1(c)], these island-like oxides were Cu_2O; such findings are in good agreement with previous results that growth of Cu oxide proceeds through formation of oxide islands [2]. Regarding area A marked in the Fig. 1(a), where the surface color does not indicate a substantial change, the Raman spectrum of Cu_2O was also detected at a relatively low intensity; suggesting that some smaller Cu_2O islands formed, such as the small islands in the inset of Fig. 1(b). Regarding He^+-implanted Cu, some

isolated dark dots were observed in the optical images [Fig. 1(d)]; they were in the form of a leaf-like structure [refer to the SEM image in Fig. 1(e)]. The Raman results in Fig. 1(f) demonstrate that these leaf-like oxides were CuO, rather than the Cu_2O that formed on pristine Cu [Fig. 1(b)]. Furthermore, the Raman spectrum of area A marked in Fig. 1(d) (where no CuO formed) indicates the characteristic peaks of Cu_2O, suggesting that Cu_2O should also form on the Cu surface. However, in the SEM image of Fig. 1(e), the surface of He^+-implanted Cu was relatively smooth (except the CuO), and there was no obvious island-like structure [Fig. 1(e)].

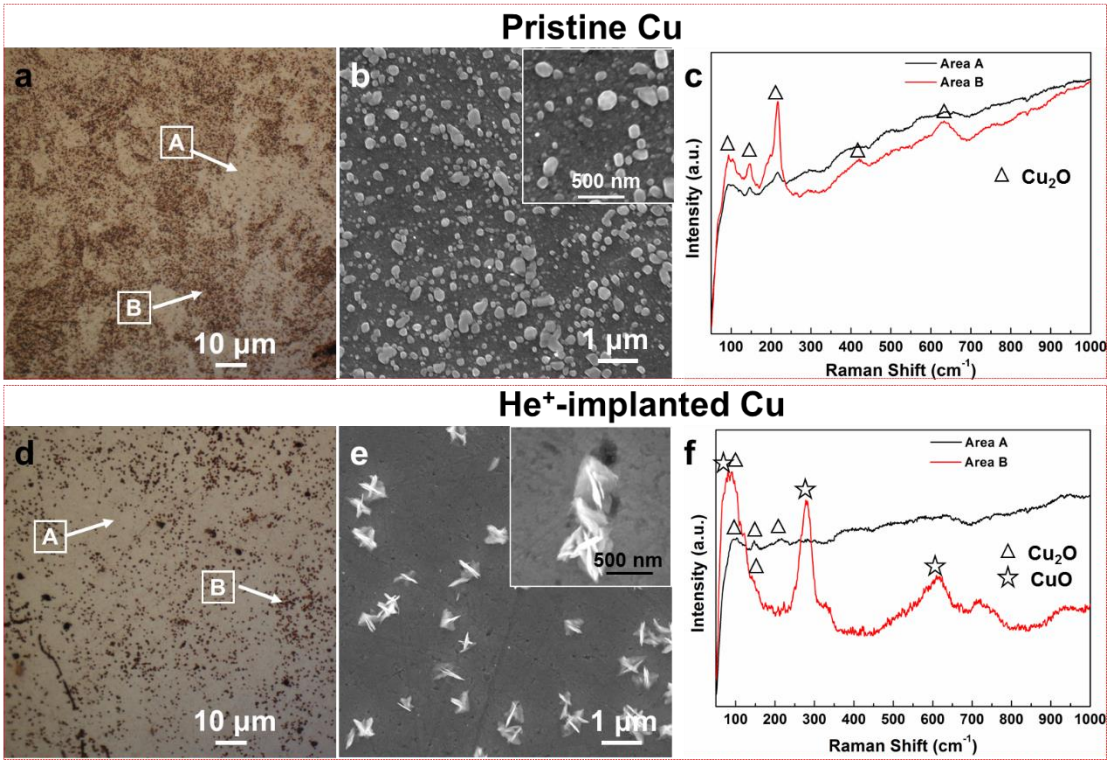

Fig. 1. (a, d) Optical images, (b, e) SEM images, and (c, f) Raman spectra of (a–c)

pristine Cu and (d–f) He^+-implanted Cu in 0.1 M aqueous NaOH for 5 h. The insets in (b, d) are the SEM images at a higher magnification. The spectra in (c) and (f) correspond to the marked areas in (a) and (d), respectively.

Upon increasing the immersion time in aqueous NaOH, the evolution of the surface morphology and oxidation products of pristine Cu were analyzed by SEM (Fig. 2) and Raman microscopy (Fig. 3). In Figs. 2(a)–2(c), the Cu_2O islands gradually increased in size via coalescence of oxide islands with increasing oxidation time. Up to 50 h, the oxidation products on pristine Cu were mainly Cu_2O [Fig. 3(a)]. In addition, the areas without large Cu_2O islands also became rougher with increasing oxidation time [Figs. 2(a)–2(c), insets]; these results are attributable to the formation and coalescence of smaller Cu_2O islands, and corrosion (or dissolution) of the Cu surface [21]. After immersion in NaOH for 55 h, some small leaf-like oxides (size: about 200 nm) were evident on pristine Cu [Fig. 2(d)]; these oxides were identified as CuO by Raman microscopy [Fig. 3(b)]. The newly generated CuO gradually increased to a size of about 1 μm after immersion in 0.1 M NaOH for 65 h [Fig. 2(e)]. However, the size of these

198 leaf-like CuO structures remained about 1 μm after immersion in NaOH for
199 80 h [Fig. 2(f)], suggesting that the growth in size of the CuO decreased or
200 even stopped after a certain duration of oxidation.

201 Regarding He^+-implanted Cu, compared with that in Fig. 1(e), more CuO
202 nucleated on the Cu surface with increasing oxidation time up to 10 h [Figs.
203 4(a) and 4(c)], with a size of about 500 nm. Over the subsequent 5 h, the
204 CuO rapidly increased in size up to about 2 μm [Figs. 4(b) and 4(c)]. The
205 shape of CuO generated on pristine Cu and He^+-implanted Cu was similar.
206 However, the CuO generated on He^+-implanted Cu exhibited a faster
207 growth rate (in terms of the final size) than that on pristine Cu. Thus, it is
208 clear that He^+ implantation can modify the oxidation behavior of Cu in 0.1
209 M NaOH, such as in terms of the faster initial generation and higher growth
210 rate of CuO.

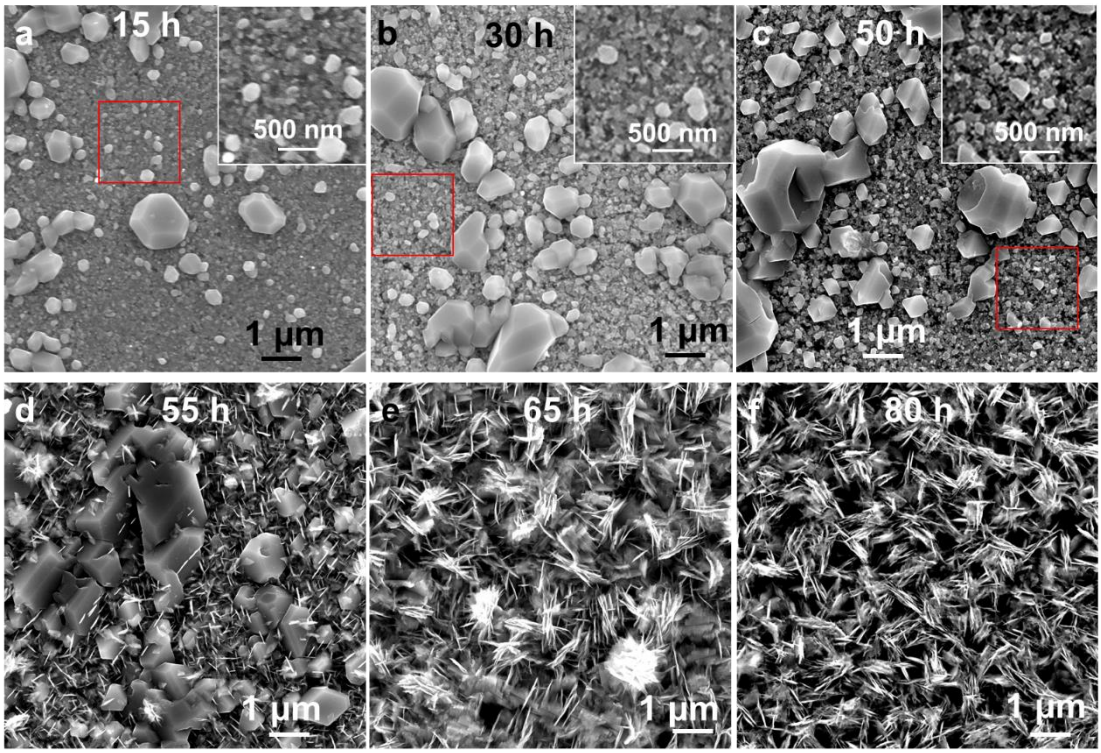

211

212 Fig. 2. SEM image of pristine Cu after immersion in 0.1 M aqueous NaOH for (a) 15 h,

213 (b) 30 h, (c) 50 h, (d) 55 h, (e) 65 h, and (f) 80 h. The insets in (a–c) are the enlarged

214 images of the marked areas in the corresponding images.

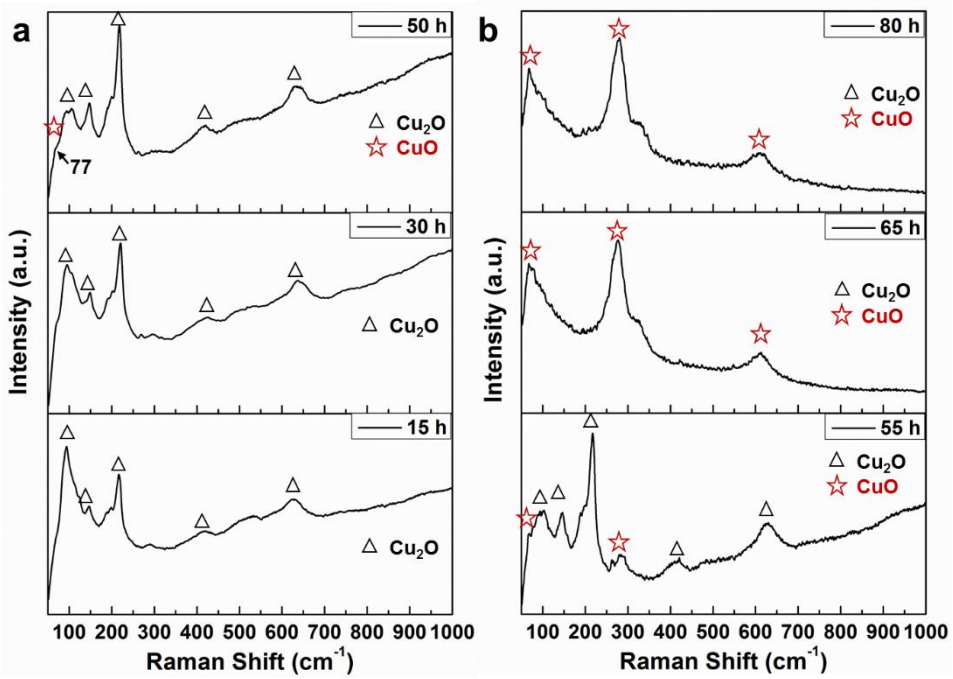

Fig. 3. Raman spectra of pristine Cu after immersion in 0.1 M aqueous NaOH for various periods of time. (a) 15–50 h. (b) 55–80 h.

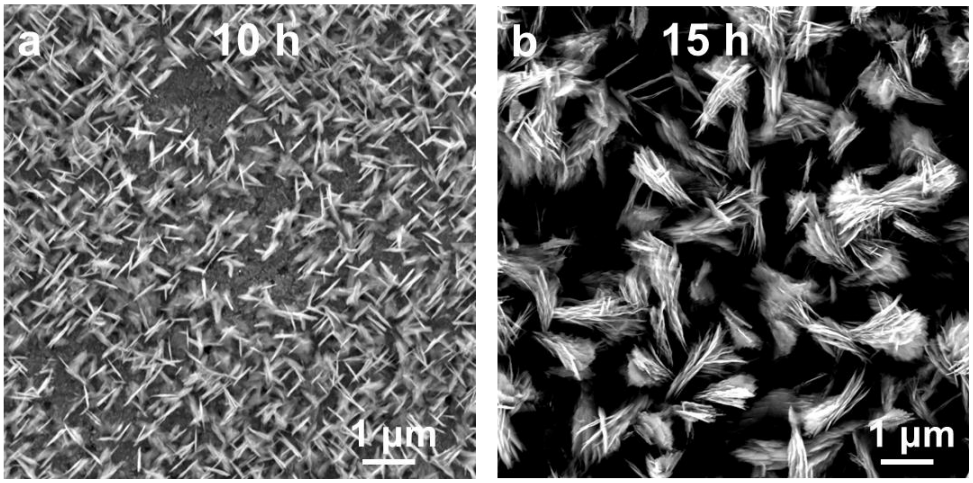

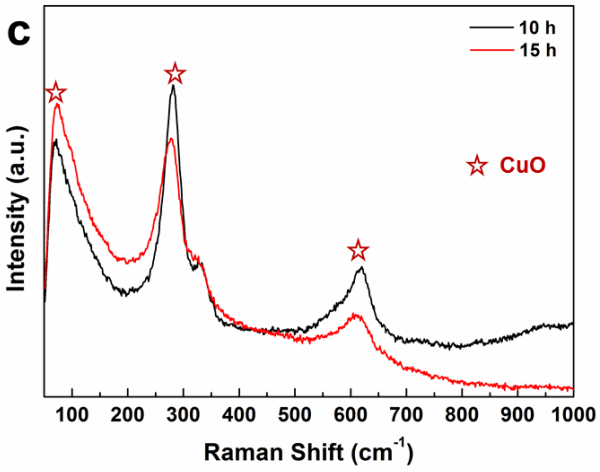

Fig. 4. SEM image of He^+-implanted Cu after immersion in 0.1 M aqueous NaOH for (a) 10 h and (b) 15 h, and (c) corresponding Raman spectra.

3.2 Fast initial generation of CuO on He^+-implanted Cu

By an XPS-etch analysis, the C content profile in depth of the Cu with or without He^+ implantation was detected in this study. A higher content and deeper distribution of C was observed in He^+-implanted Cu than that in pristine Cu [Fig. 5(a)], indicating that additional C was introduced into this sample to a depth of about 6 nm during He^+ implantation. A small quantity of C was also detected on the surface of pristine Cu, which is attributable to the dust in the air that was absorbed onto the Cu surface, which was usually detected by XPS analysis. By TEM, a film was observed that covered the surface of He^+-implanted Cu [Fig. 5(b)]; which should correspond to the

C-containing barrier layer [20].

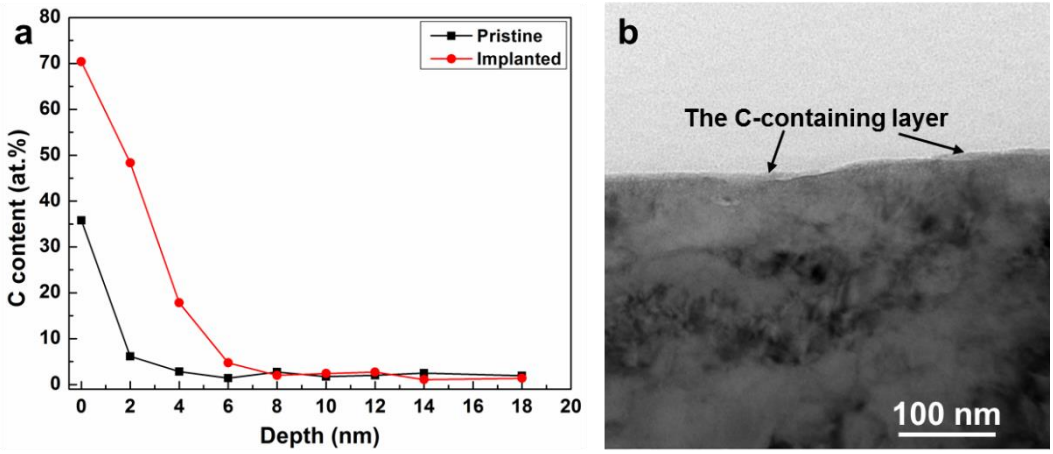

Fig. 5. (a) C content profile in depth detected by X-ray photoelectron spectroscopy etching for the samples with and without He^+ implantation. (b) Cross-sectional transmission electron microscopy image of He^+-implanted Cu with a fluence of 5×10^{15} cm^{-2}.

In alkaline solution, the formation of Cu oxide is a two-step growth process and can be described as follows [23,24]:

$$2Cu + 2OH^- \rightarrow Cu_2O + H_2O + 2e^- \quad (1)$$

$$Cu_2O + 2OH^- \rightarrow 2CuO + H_2O + 2e^- \quad (2)$$

Furthermore, generation of CuO usually occurs after formation of a continuous Cu_2O film on the Cu substrate [21,24]. By TEM, the evolution of the surface morphology on pristine Cu was observed (Fig. 6). For

pristine Cu in 0.1 M NaOH for 5 h [Fig. 6(a)], the oxidation state along the Cu surface was inhomogeneous, with some areas covered with Cu_2O islands and some areas not covered. After immersion in NaOH for 30 h, islands on the Cu surface enlarged via coalescence of the islands, but there were still some areas that were not covered by Cu_2O islands [Fig. 6(b)]. By increasing the oxidation time to 50 h, a continuous Cu_2O film was observed on the Cu [Fig. 6(c)]. Over the 5 h after formation of this Cu_2O film, leaf-like CuO was evident [Fig. 2(d)]. These results agree well with previous reports that the generation of CuO usually occurs after formation of a continuous Cu_2O film [24]. Meanwhile, although the whole surface of pristine Cu is covered by the Cu_2O film after immersion in NaOH for 55h, the nucleation of CuO is not homogeneous as show in the Fig. 2(d). More CuO preferentially nucleated at the area with a thin oxide film (i.e. without large Cu_2O island) [Fig. 2(d)], which suggests that a thinner oxide film could accelerate the generation of CuO.

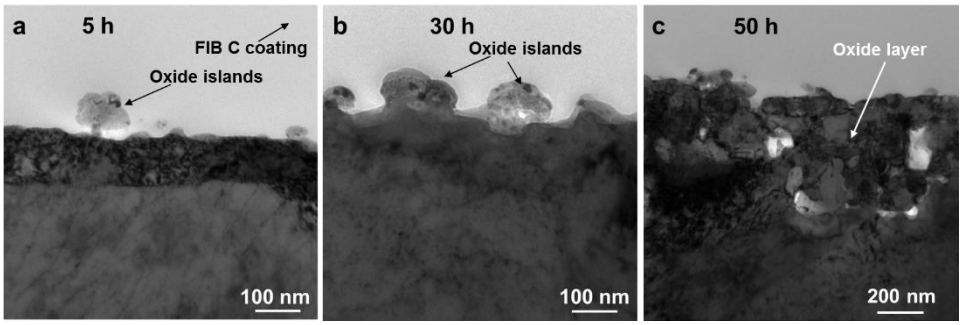

Fig. 6. Cross-sectional bright-field TEM image of pristine Cu after immersion in 0.1 NaOH for (a) 5 h, (b) 30 h, and (c) 50 h.

Regarding He^+-implanted Cu after immersion in 0.1 NaOH for 5 h, a film was observed on the Cu surface in the bright-field TEM images [Fig. 7(a)], with a thickness of about 20 nm. In accordance with observations by HAADF–STEM in Fig. 7(b), this film exhibited a comparatively weaker bright contrast than that of the Cu substrate. HAADF–STEM images are sensitive to the atomic number (z) of the sample; i.e., heavier-element atoms exhibit a brighter contrast. Thus, this layer structure should have a lower atomic mass than that of Cu [25]. In accordance with detection by STEM–EDS, the O/Cu atomic ratio in areas 1 and 2 was close to that of Cu_2O. By also considering the Raman results in Fig. 1(f), Cu_2O formed on the Cu surface; i.e., Cu_2O was present in this film. These results indicate that to some extent a Cu_2O film already formed on He^+-implanted Cu after

immersion in 0.1 M aqueous NaOH for 5 h. Considering that a Cu_2O film usually must form before generation of CuO, and that CuO preferentially nucleate at the area with a thinner oxide film [Fig. 2(d)], the rapidly formed Cu_2O thin film should account for the faster initial generation of CuO on He^+-implanted Cu [Fig. 1(e)].

The boundary between different oxide particles was observed in this oxide film [Figs. 7(a) and 7(b), such as the area marked by a red circle in Fig. 7(a)], suggesting that this film also formed through coalescence of oxide particles. To better understand the evolution of oxide in He^+-implanted Cu, an oxidation experiment over a briefer period of time was carried out for this sample [Figs. 7(c) and 7(d)]. Some small oxide particles (about 15 nm in thickness) were observed on He^+-implanted Cu after immersion in 0.1 M NaOH for 2 h [Fig. 7(c)], which gradually grew into a small oxide film with increasing oxidation time to 3 h [Fig. 7(d)]. This result confirms the following: the oxide film that formed on He^+-implanted Cu proceeded through coalescence of oxide particles. Compared with that of the oxide islands on pristine Cu [Fig. 6(a)], the thickness of this oxide film on He^+-implanted Cu [Fig. 7(a)] was thinner,

suggesting that lengthways growth of oxide on He^+-implanted Cu was limited. Furthermore, the evolution of oxide on He^+-implanted Cu [Figs. 7(a), 7(c), and 7(d)] implies a rapid lateral growth of oxide through coalescence of oxide particles. Thus, the rapid formation of a thin oxide film on He^+-implanted Cu is attributable to the limited lengthways growth and enhanced lateral growth of the oxide.

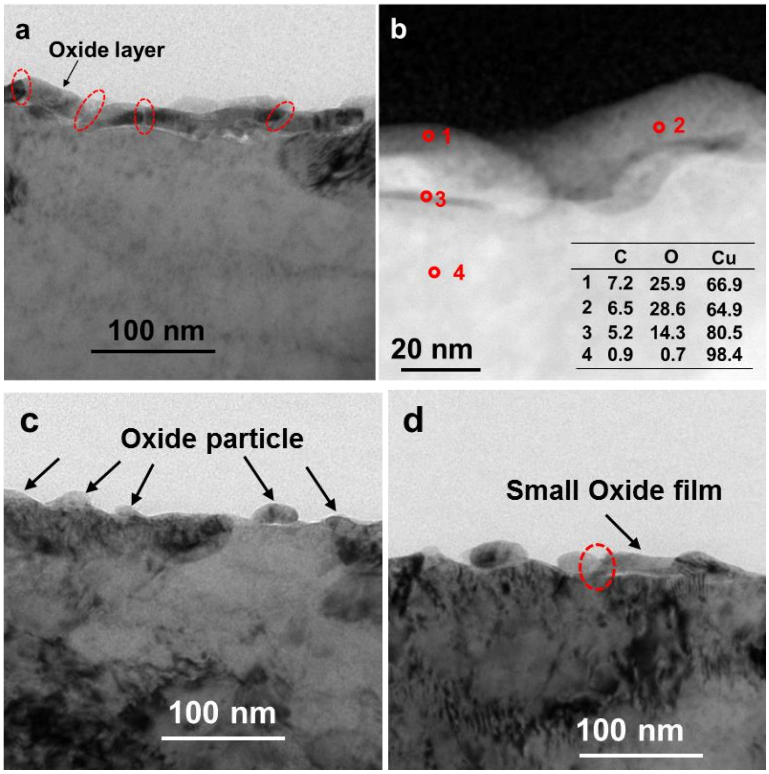

Fig. 7. (a) Cross-sectional bright-field TEM image and (b) HAADF-STEM image of He^+-implanted Cu after immersion in 0.1 M NaOH for 5 h. The table inset in (b) is the STEM–EDS results of the corresponding area. (c and d) Cross-sectional bright-field TEM image of He^+-implanted Cu after immersion in 0.1 M NaOH for (c) 2 h and (d) 3

h.

To better understand the formation of this oxide film on He^+-implanted Cu, the microstructure of this film was analyzed by HR–TEM. In Fig. 8(a), the fast-Fourier transform (FFT) of a selected area around the oxide film and Cu substrate indicated a ring pattern of amorphous C (Am. C). By the inverse fast-Fourier transform (IFFT) technique, there was C in this oxide film [Fig. 8(b)]; with some C concentrated at the upper surface of the oxide film, and the interface between the oxide film and Cu substrate [marked by the dashed yellow line in the Fig. 8(a)]. These results agree well with the C content profile in depth detected by XPS-etching techniques [Fig. 8(c)]. Because no additional C entered the sample during oxidation, the C in the oxide film is attributable to the C introduced during He^+ implantation (Fig. 5). For a comparison, Fig. 8(d) shows a HR–TEM image of Cu_2O islands on pristine Cu after immersion in NaOH for 5 h. There was no C-concentrated layer around the interface between the Cu oxide and Cu substrate. Oxidation of Cu in an aqueous environment implies electronic exchanges (electrochemical reactions) and ionic species transport between the base metal and environment, and it has been demonstrated that the

presence of C passivated Cu oxidation [20, 26]. In the present study, C was concentrated at the upper surface of the oxide film (and the interface between the oxide film and Cu substrate) on He^+-implanted Cu after immersion in NaOH for 5 h. Thus, the limited the lengthways growth of the oxide in He^+-implanted Cu should be mainly attributed to the C (introduced during He^+ implantation). Furthermore, Cu oxide more-readily nucleates and increases in size at regions with surface defects [2,12]. These processes might facilitate establishment of an oxide film; accelerated formation of an oxide film was observed on Ar^+-implanted Cu due to surface defects induced by ion implantation [20]. In this study, because of ion sputtering, surface defects are also expected to be introduced by He^+ implantation. By a comparison of Figs. 6(a) and 7(c), more oxide nuclei formed on He^+-implanted Cu than on pristine Cu over the initial oxidation period because of surface defects; resulting in enhanced lateral growth of Cu oxide via coalescence of Cu oxide particles and rapid formation of an oxide film.

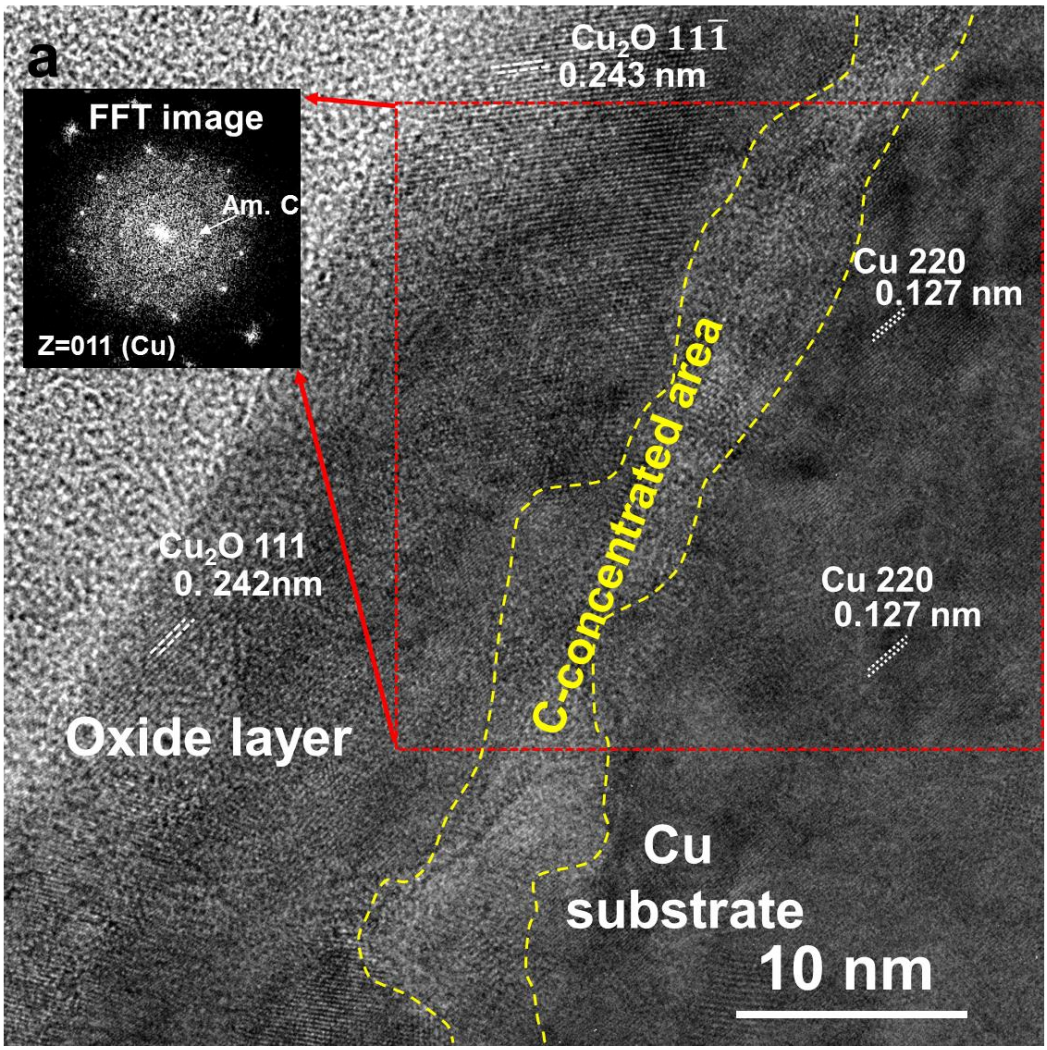
a
FFT image
Am. C
Z=011 (Cu)
Cu_2O 111
0.243 nm
Cu 220
0.127 nm
C-concentrated area
Cu_2O 111
0. 242nm
Cu 220
0.127 nm
Oxide layer
Cu
substrate
10 nm

341

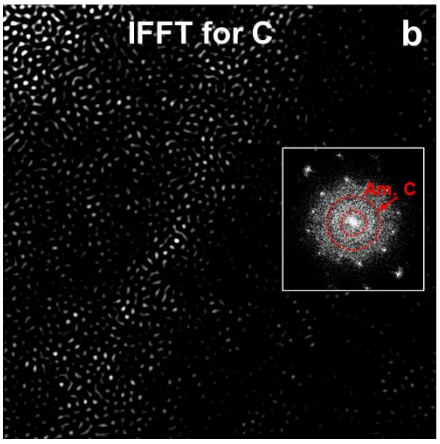
IFFT for C
b
Am. C

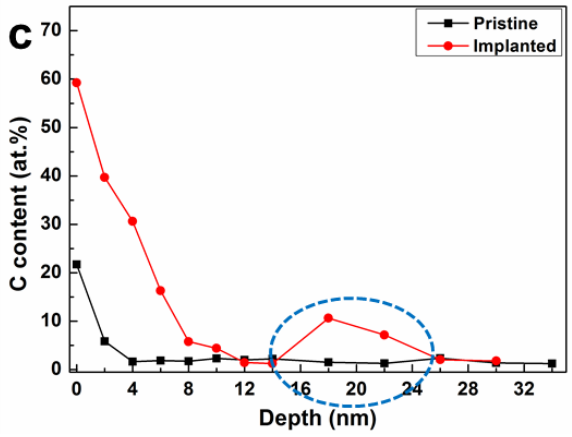
c
Pristine
Implanted
C content (at.%)
Depth (nm)
0
10
20
30
40
50
60
70
0
4
8
12
16
20
24
28
32

342

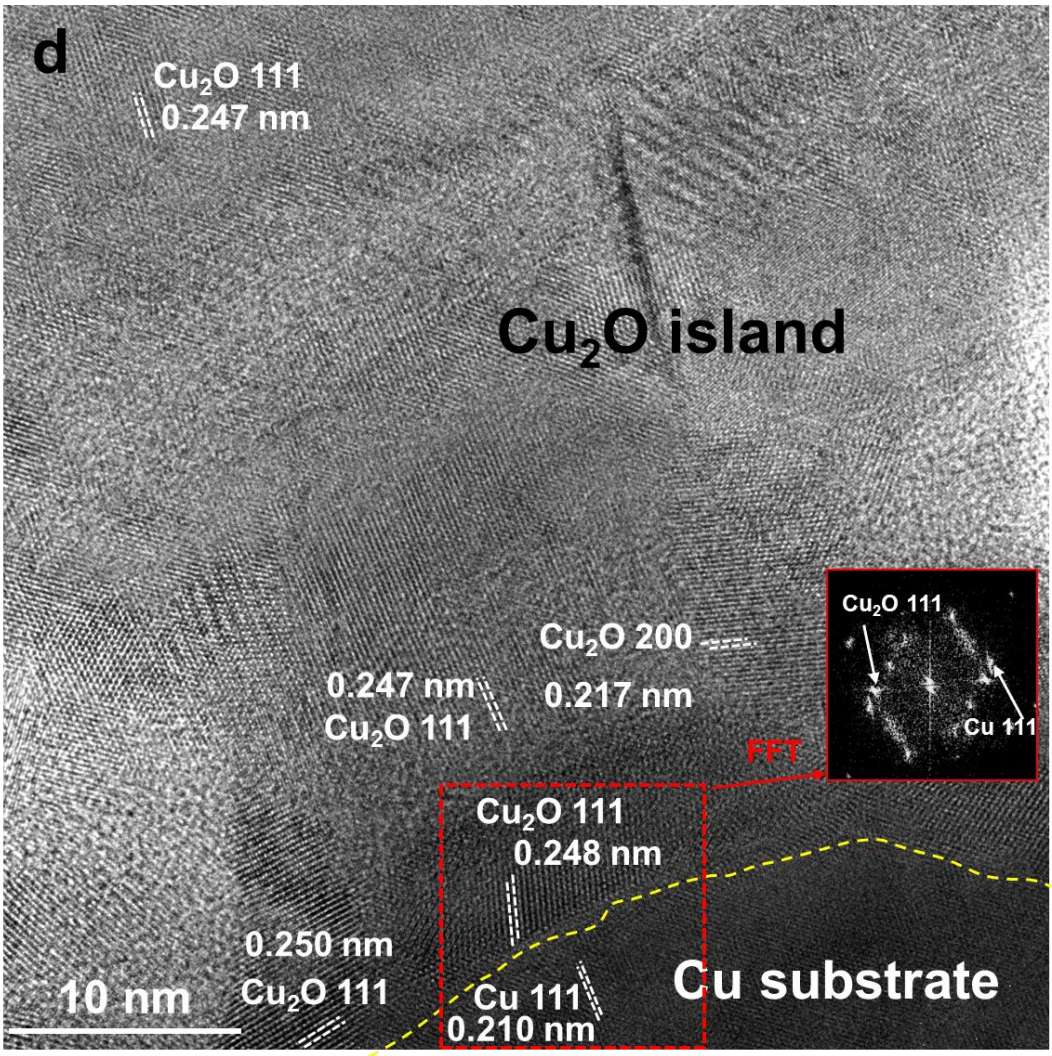

Fig. 8. (a) HR-TEM image of an oxide layer on He^+-implanted Cu. The inset is a FFT image of the selected area marked by a red square. (b) IFFT for C of the selected area in (a). (c) C content profile in depth detected by XPS etching; corresponding spectra provided in Fig. S3. (d) HR-TEM image of Cu_2O islands on pristine Cu after immersion in 0.1 M NaOH for 5 h.

3.3 Rapid growth of CuO on He^+-implanted Cu

After formation of a Cu_2O layer, leaf-like CuO was generated on both pristine Cu [55 h; Fig. 2(d)] and He^+-implanted Cu (5 h; Fig. 1(d)]. The configuration of CuO on the surface was observed by TEM and HAADT–STEM (Fig. 9, pristine Cu; and Fig. 10, He^+-implanted Cu). In Fig. 9(a), three layers were distinguished by image contrast and selected-area electron diffraction: i.e., the top CuO layer, middle Cu_2O layer, and bottom Cu substrate; confirmed by STEM–EDS [Fig. 9(b)]. The thickness of the Cu_2O layer in pristine Cu was about 300 nm [Fig. 10(a)]. However, in He^+-implanted Cu, there was no obvious Cu_2O layer by relatively low-magnification TEM and selected-area electron diffraction [Fig. 10(a)]. By STEM–EDS, the composition of various areas was detected [Fig. 10(b)]; the area around the boundary of Cu and CuO [black square in Fig. 10(b)] was analyzed by HR–TEM. A thin Cu_2O layer with a thickness of about 4 nm formed between the Cu and CuO, which was substantially thinner than that on pristine Cu [about 300 nm in Fig. 9(a)].

In Figs. 9 and 10, double oxide layers were confirmed on both pristine Cu and He^+-implanted Cu, with an outer layer of leaf-like CuO and an inner layer of Cu_2O. However, the Cu_2O layer that formed on

He^+-implanted Cu was much thinner than that on pristine Cu. Oxidation of Cu in an aqueous environment proceeds with ionic species transport between the base metal and environment. A dense Cu_2O layer can hinder growth of CuO by blocking ionic species transport between the Cu and solution [21,22,24]. Therefore, the more-rapid growth of CuO on He^+-implanted Cu (Fig. 4) than that on pristine Cu [Figs. 2(d)–2(f)] is mainly attributable to the thinner Cu_2O layer on the former. In addition, the lower number density of CuO [Figs. 4(b) and 2(f)] might also contribute to the higher growth rate of CuO on He^+-implanted Cu compared with that on pristine Cu.

The growth of CuO slowed after immersion in 0.1 M NaOH for 65 h [Figs. 2(e) and 2(f)], which was also observed in anodization synthesis of CuO [24]. By comparing the Cu_2O layer in Figs. 5(c) and 9(a), the porous Cu_2O layer became more compact with increasing oxidation time [Fig. 9(a)]. The denser Cu_2O layer can block direct contact of the Cu substrate with the solution, and decrease the transport of ionic species between them [21]; resulting in a decreased growth rate of CuO on pristine Cu.

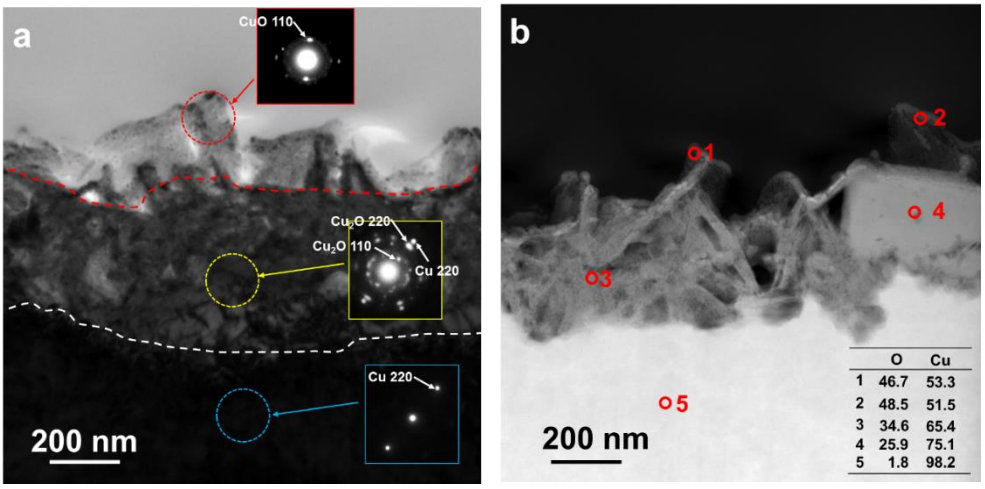

386

387 Fig. 9. (a) Cross-sectional bright-field TEM image and (b) HAADF-STEM image of

388 pristine Cu after immersion in NaOH for 55 h. The table inset in (b) shows the STEM–

389 EDS results of the corresponding area.

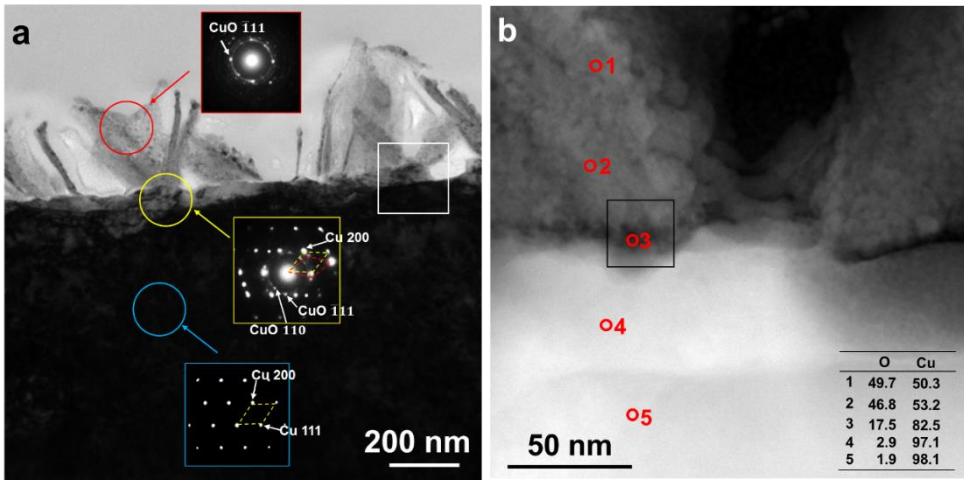

390

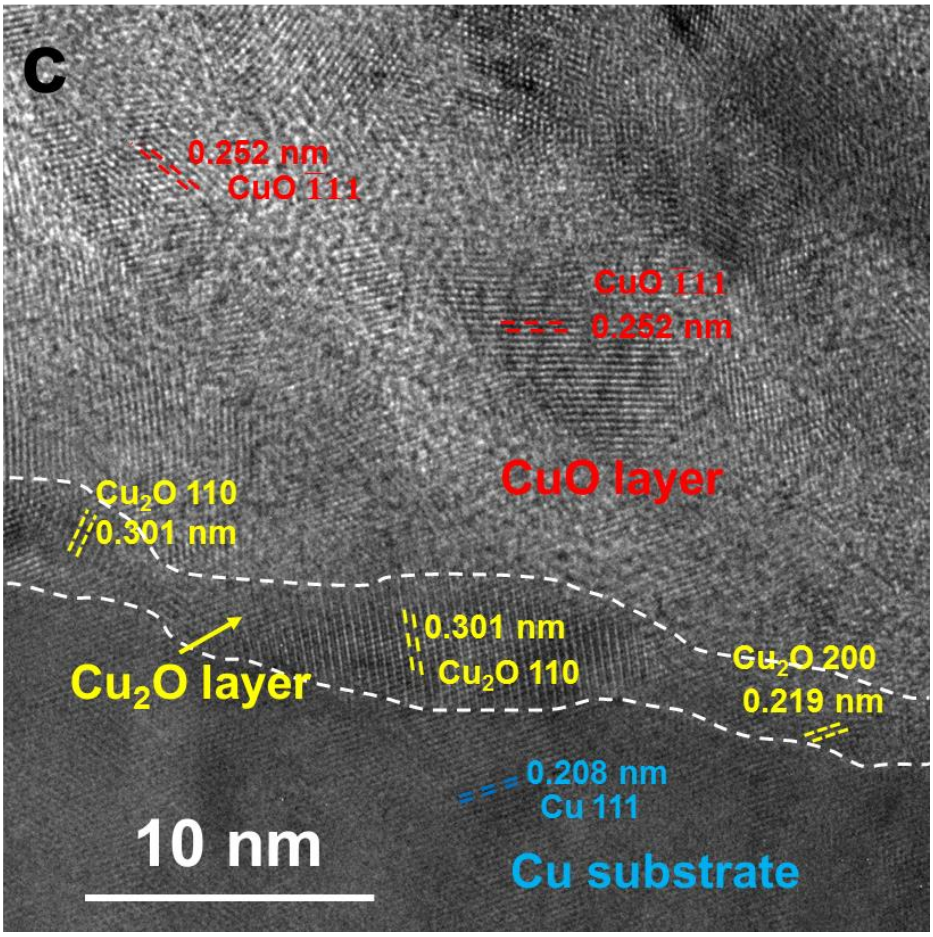

391

392 Fig. 10. (a) Cross-section bright-field TEM image and HAADF-STEM image of
393 He^+-implanted Cu after immersion in NaOH for 10 h. The table inset in (b) is the
394 STEM–EDS results of the corresponding area. (c) HR-TEM image around the Cu/CuO
395 interface.

396

397 3.4 Potential applications of ion implantation in the Cu oxidation

398 In our previous studies, the C-containing barrier layer that formed on
399 He^+-implanted Cu passivated Cu thermal oxidation [20]. However, in this

study, the C (introduced during He^+ implantation) accelerated generation and growth of CuO on He^+-implanted Cu; resulting in a heavier oxidation state on He^+-implanted Cu than that on pristine Cu in alkaline aqueous solution. However, during the initial oxidation period (in NaOH for 5 h), the C-containing layer limited the lengthways growth of oxide on He^+-implanted Cu [Fig. 7(a)]; which implies that a thicker C-containing layer might result in a stronger passivation effect on Cu oxidation. Furthermore, the modified Cu oxidation induced by He^+ implantation also suggests that ion implantation might be useful to modify CuO growth.

CuO is an important semiconductor that is used in photoelectronic, catalytic, and solar energy technologies [2,27]. Various studies have been performed to exploit and develop appropriate methods for Cu oxide nanostructure growth [28,29]; such as increasing the efficiency by decreasing the fabrication time [22], preparing highly ordered arrays of Cu oxide nanostructures [8,24], and low-cost fabrication by photosynthesis [29]. However, to date, developing commercially viable copper oxides used for photocatalytic and sensor applications remains challenging. In this study, a faster initial generation and more-rapid growth of CuO was

418 achieved by implanting some C into the Cu surface by He^+ implantation;
419 which suggests that ion implantation, such as C^+ implantation, might be
420 used to decrease the time or energy cost for fabricating CuO. Furthermore,
421 regarding pristine Cu, a rough and loose surface was formed before
422 generating CuO [Fig. 2(c)]; resulting in a disordered distribution of CuO on
423 the Cu substrate [Figs. 2(f) and 11(a)]. However, regarding He^+-implanted
424 Cu, the surface of the Cu substrate after forming CuO was still relatively
425 smooth [Figs. 10(a) and 11(b)]; corresponding to a relatively uniform and
426 ordered distribution of CuO. This indicates that the configuration of CuO
427 on the Cu support was modified by ion implantation. Overall, both the
428 more-rapid growth of CuO and the ordered distribution of CuO induced by
429 He^+ implantation suggests that shallow ion implantation, such as that by
430 He^+ or C^+, can be used to modulate CuO growth. In addition, the modified
431 configuration by He^+ implantation may lead to some revisions of optical or
432 electrical properties of CuO film. The difference between the pristine
433 sample and He^+-implanted sample in term of the bonding strength of CuO
434 film and substrate and optical absorption property of CuO is shown in the
435 supplementary. More investigations about the revised properties of CuO

436 will be performed in the future.

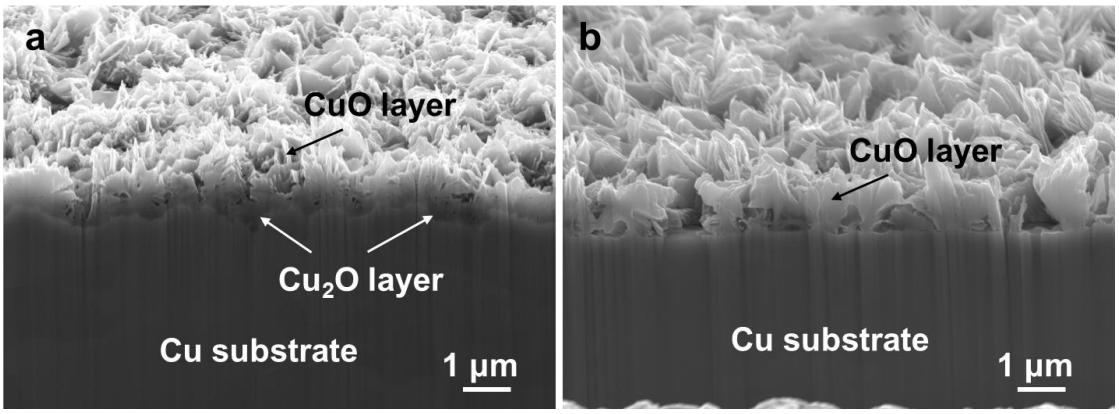

437

438 Fig. 11. Cross-sectional SEM image, viewed at a tilt angle of 70°. (a) Pristine Cu after

439 immersion in 0.1 M NaOH for 80 h. (b) He^+-implanted Cu after immersion in 0.1 M

440 NaOH for 15 h.

441

442 **5. Conclusions**

443 The oxidation behavior of He^+-implanted Cu in 0.1 M aqueous NaOH

444 was investigated. Because of He^+ implantation, and the C that was

445 concomitantly implanted into the Cu surface (which originated from the

446 pump oil within the vacuum system), accelerated oxidation was observed in

447 reference to the faster initial generation and more-rapid growth of CuO.

448 Furthermore, He^+ implantation rendered the distribution of the CuO on the

449 Cu substrate relatively uniform and ordered. The more-rapid growth and

450 uniform distribution of CuO induced by He^+ implantation suggests that ion

implantation can be used to modulate the fabrication of CuO nanostructures.

Acknowledgments

This work was supported by JSPS KAKENHI grant numbers JP19K22035 and JP19H00799. Part of this work was conducted at the Joint-Use Facilities at Hokkaido University, supported by the Project for Promoting Public Utilization of Advanced Research Infrastructure (Program for Supporting Introduction of the New Sharing System) under grant number JPMXS0420100519 and by the Nanotechnology Platform program of the Ministry of Education, Culture, Sports, Science and Technology (MEXT), Japan. The authors thank Mr. R. Ota for help with STEM analyses. Dr. Yang acknowledges stipend support from the Chinese Scholarship Council to perform this work at Hokkaido University. We acknowledge Dr. Takashi Sakamura in Industrial Research Institute of Local Independent Administrative Agency Hokkaido Research Organization for his help of in the scratch testing. The sponsors had no role in study design; in the collection, analysis, and interpretation of data; in the writing of the report;

and in the decision to submit the article for publication. We thank Michael Scott Long, PhD, from Edanz (https://jp.edanz.com/ac) for editing a draft of this manuscript.

References

[1] J. Peng, B. Chen, Z. Wang, J. Guo, B. Wu, S. Hao, Q. Zhang, L. Gu, Q. Zhou, Z. Liu, S. Hong, S. You, A. Fu, Z. Shi, H. Xie, D. Cao, C. Lin, G. Fu, L. Zheng, Y. Jiang, N. Zheng, Surface coordination layer passivates oxidation of copper, Nature, 586 (2020) 390-394. https://doi.org/10.1038/s41586-020-2783-x.

[2] A. M. C. Gattinoni, Atomistic details of oxide surfaces and surface oxidation: the example of copper and its oxides, Surf. Sci. Rep. 70 (2015) 424–447. https://doi.org/10.1016/j.surfrep.2015.07.001.

[3] D. Kang, J. Y. Kwon, H. Cho, J. Sim, H. S. Hwang, C. S. Kim, Y. J. Kim, R. S. Ruoff, H. S. Shin, Oxidation resistance of iron and copper foils coated with reduced graphene oxide multilayers, ACS Nano. 6 (2012) 7763–7769. https://doi.org/10.1021/nn3017316.

[4] X. Q. Zhao, Modification of oxidation resistance of copper films by shallow implantation, J. Appl. phys. 90 (2001) 1638–1641. https://doi.org/10.1063/1.1379774.

[5] L. Wu, L. Tsui, N. Swami, G. Zangari, Photoelectrochemical stability of electrodeposited Cu_2O films, J. Phys. Chem. C 114 (2010) 11551–11556. https://doi.org/10.1021/jp103437y.

[6] Y. Li, S. Chang, X. Liu, J. Huang, J. Yin, G. Wang, D. Cao, Nanostructured CuO directly grown on copper foam and their supercapacitance performance, Electrochim. Acta 85 (2012) 393–398. https://doi.org/10.1016/j.electacta.2012.07.127.

[7] Y. Yu, Y. Shi, C. Chen, Nanoporous cuprous oxide/lithia composite anode with capacity increasing characteristic and high rate capability, Nanotechnology 18 (2007) 55706. Https://doi:10.1088/0957-4484/18/5/055706.

[8] L. Ma, Y. Lin, Y. Wang, J. Li, E. Wang, M. Qiu, Y. Yu, Aligned 2-D nanosheet Cu_2O film: oriented deposition on Cu foil and its photoelectrochemical property, J. Phys. Chem. C 112 (2008) 18916–18922. https://doi.org/10.1021/jp807219u.

[9] Y. Mao, J. He, X. Sun, W. Li, X. Lu, J. Gan, Z. Liu, L. Gong, J. Chen, P. Liu, Y. Tong, Electrochemical synthesis of hierarchical Cu_2O stars with enhanced photoelectrochemical properties, Electrochim. Acta 62 (2012) 1–7. https://doi.org/10.1016/j.electacta.2011.10.106.

[10] J. Zhang, Y. Wang, C. Yu, X. Shu, L. Jiang, J. Cui, Z. Chen, T. Xie, Y. Wu, Enhanced visible-light photoelectrochemical behaviour of heterojunction composite

505 with Cu_2O nanoparticles-decorated TiO_2 nanotube arrays, New J. Chem. 38 (2014) 4975.
506 https://doi: 10.1039/c4nj00787e.
507 [11] S. Zhang, S. Zhang, F. Peng, H. Zhang, H. Liu, H. Zhao, Electrodeposition of
508 polyhedral Cu_2O on TiO_2 nanotube arrays for enhancing visible light photocatalytic
509 performance, Electrochim. Commun. 13 (2011) 861–864.
510 https://doi.org/10.1016/j.elecom.2011.05.022.
511 [12] C. J. McHargue, Ion implantation in metals and ceramics, International Metals
512 Reviewers 31 (1986) 49–76. https://doi.org/10.1179/imtr.1986.31.1.49
513 [13] Y. Zhang, W. J. Weber, Ion irradiation and modification: The role of coupled
514 electronic and nuclear energy dissipation and subsequent nonequilibrium processes in
515 materials, Appl. Phys. Rev. 7 (2020) 41307. https://doi.org/10.1063/5.0027462.
516 [14] D. Q. Peng, X. D. Bai, X. W. Chen, Q. G. Zhou, X. Y. Liu, R. H. Yu, Aqueous
517 corrosion behavior of zirconium subjected to high-energy krypton-ion bombardment,
518 Appl. Surf. Sci. 227 (2004) 73–80. https://doi.org/10.1016/j.apsusc.2003.11.001.
519 [15] L. A. Luiz, B. C. E. S. Kurelo, G. B. de Souza, J. de Andrade, C. E. B. Marino,
520 Effect of nitrogen plasma immersion ion implantation on the corrosion protection
521 mechanisms of different stainless steels, Mater. Today Commun. 28 (2021) 102655.
522 https://doi.org/10.1016/j.mtcomm.2021.102655.

523 [16] C. M. Abreu, M. J. Cristóbal, R. Figueroa, G. Pena, Influence of molybdenum ion
524 implantation on the localized corrosion resistance of a high strength aluminium alloy,
525 Corros. Sci. 54 (2012) 143–152. https://doi.org/10.1016/j.corsci.2011.09.003.
526 [17] Z. Qin, Q. Luo, Q. Zhang, Z. Wu, L. Liu, B. Shen, W. Hu, Improving corrosion
527 resistance of nickel-aluminum bronzes by surface modification with chromium ion
528 implantation, Surf. Coat. Technol. 334 (2018) 402–409.
529 https://doi.org/10.1016/j.surfcoat.2017.11.066.
530 [18] A. J. Kellock, M. H. Tabacniks, J. E. E. Baglin, N. S. Somcio, T. T. Bardin, D. C.
531 Miller, Mechanism for ion beam passivation of copper surfaces, Nucl. Instrum. Methods
532 Phys. Res. B 127/128 (1997) 742-746.
533 https://doi.org/10.1016/S0168-583X(96)01169-X.
534 [19] E. H. Hirsch, The growth of carbonaceous contamination on surfaces undergoing
535 ion bombardment, J. Phys. D: Appl. Phys. 10 (1977) 2069.
536 https://iopscience.iop.org/article/10.1088/0022-3727/10/15/010/meta.
537 [20] S. Yang, Y. Nakagawa, T. Shibayama, An investigation of surface contamination
538 introduced during He+ implantation and subsequent effects on the thermal oxidation of
539 Cu, Appl. Surf. Sci. 579 (2022) 152163. https://doi.org/10.1016/j.apsusc.2021.152163.
540 https://doi.org/10.1016/j.corsci.2021.109471.

[21] J. Wu, Y. Wu, J. Wang, Comparative study on corrosion behavior of Cu and Sn under UV light illumination in chloride-containing borate buffer solution, Corros. Sci. 186 (2021) 109471.

[22] S. Anantharaj, H. Sugime, S. Noda, Ultrafast growth of a $Cu(OH)_2$-CuO nanoneedle array on Cu foil for methanol oxidation electrocatalysis, ACS Appl. Mater. Interfaces 12 (2020) 27327–27338. https://doi.org/10.1021/acsami.0c08979.

[23] J. Y. Zheng, T. K. Van, A. U. Pawar, C. W. Kim, One-step transformation of Cu to Cu_2O in alkaline solution, RSC Adv. 4 (2014) 18616. https://doi: 10.1039/c4ra01174k.

[24] X. Shu, H. Zheng, G. Xu, J. Zhao, L. Cui, J. Cui, Y. Qin, Y. Wang, Y. Zhang, Y. Wu, The anodization synthesis of copper oxide nanosheet arrays and their photoelectrochemical properties, Appl. Surf. Sci. 412 (2017) 505–516. https://doi.org/10.1016/j.apsusc.2017.03.267.

[25] S. Yang, Y. Nakagawa, M. Kondo, T. Shibayama, Anisotropic defect distribution in He^+-irradiated 4H-SiC: Effect of stress on defect distribution, Acta Material. (211) 116845. https://doi.org/10.1016/j.actamat.2021.116845.

[26] Y. Ziat, M. Hammi, Z. Zarhri, C. Laghlimi, Epoxy coating modified with graphene: A promising composite against corrosion behavior of copper surface in marine media, J. All. s Comp. 820 (2020) 1533802. https://doi.org/10.1016/j.jallcom.2019.153380.

559 [27] S. Anantharaj, S. R. Ede, K. Sakthikumar, K. Karthick, S. Mishra, S. Kundu,
560 Recent trends and perspectives in electrochemical water splitting with an emphasis on
561 sulfide, selenide, and phosphide catalysts of Fe, Co, and Ni: A review, ACS Catal. 6
562 (2016) 8069–8097. https://doi.org/10.1021/acscatal.6b02479.
563 [28] H. Yu, J. Yu, S. Liu, S. Mann, Template-free hydrothermal synthesis of CuO/Cu_2O
564 composite hollow microspheres, Chem. Mater. 19 (2007) 4327–4334.
565 https://doi.org/10.1021/cm070386d.
566 [29] J. Mizuno, M. Jeem, Y. Takahashi, M. Kawamoto, K. Asakura, S. Watanabe, Light
567 and shadow effects in the submerged photolytic synthesis of micropatterned CuO
568 nanoflowers and ZnO nanorods as optoelectronic surfaces, ACS Appl. Nano Mater. 3
569 (2020) 1783–1791. https://doi.org/10.1021/acsanm.9b02385.